ELSEVIER

Journal of Power Sources 104 (2002) 52–61

JOURNAL OF POWER SOURCES

www.elsevier.com/locate/jpowsour

# Characterization of hydrous ruthenium oxide/carbon nanocomposite supercapacitors prepared by a colloidal method

Hansung Kim, Branko N. Popov*

*Department of Chemical Engineering, Center for Electrochemical Engineering, University of South Carolina, Columbia, SC 29208, USA*

Received 15 June 2001; accepted 20 July 2001

**Abstract**

Amorphous nanostructured composite materials with different $RuO_2$ loadings on carbon were prepared by colloidal method. The annealing temperature was found to be critical in optimizing the electrochemical performance of this material. FT Raman study confirmed that ruthenium complex converted to ruthenium oxide after annealing at 100 °C. The specific capacitance of $RuO_2$/carbon composite electrode (40 wt.% Ru) was calculated by using cyclic voltammetry, which was to be 407 F/g. The specific capacitance of $RuO_2{\cdot}xH_2O$ was estimated to be approximately 863 F/g by subtracting the contribution of double layer capacitance resulting from carbon in the composite. Transmission electron microscopy indicated that the particle size of $RuO_2{\cdot}xH_2O$ on carbon was approximately 3 nm. By increasing the Ru loading over 60 wt.%, the particle size of $RuO_2$ increased up to several micrometers resulting in a decrease of the utilization of $RuO_2$, the specific surface area and the rate capability. 

*Keywords:* Colloidal method; Ruthenium oxide; Nanocomposite; Supercapacitors

## 1. Introduction

Amorphous ruthenium oxide is considered to be a promising material for a high energy density power source because the charge can be stored in the bulk of the amorphous material [1]. Amorphous $RuO_2{\cdot}xH_2O$ prepared by sol–gel process, showed a capacitance of over 720 F/g, which is considerably larger than that of activated carbon based electrochemical double layer capacitor [2]. However, the high material cost of $RuO_2{\cdot}xH_2O$ and low porosity which causes depletion of the electrolyte adsorbed on the electrode as well as the rapid decrease of power density observed at high charge/discharge rates make this material inadequate for commercial applications [3].

In order to reduce the cost of material and increase its high rate performance, the recent research has focused on developing structures of $RuO_2$/carbon composite materials. Miller and Dunn [4,5] deposited nanosize $RuO_2$ particle on the carbon aerogel by chemical vapor impregnation. The high annealing temperature of approximately 300 °C used in this work initiated a crystalline transition of $RuO_2$, and resulted in a specific capacitance of 330 F/g that is much lower than the specific capacitance obtained by using a sol–gel method. Zheng and Jow reported that the performance of $RuO_2$ is highly sensitive to the annealing temperature and that its structure changed from amorphous to crystalline above 175 °C [1].

Sato et al. [6] loaded amorphous $RuO_2{\cdot}xH_2O$ on the various activated carbons by sol–gel process. The results of this study indicated that the large particles made from sol–gel method blocked the mesopores in activated carbon which lowered the double layer capacitance coming from carbon.

Our studies indicated that composite Ru oxide-carbon based supercapacitors possess superior energy and power densities as compared to bare carbon [7,8]. An electroless deposition process was used to synthesize the ruthenium oxide-carbon composites. Loading a small amount of Ru oxide (9%) on carbon increases the capacitance from 98 to 190 F/g.

We developed a mathematical model that explicitly accounts for particle packing effects in composite electrochemical capacitor consisting of hydrous ruthenium oxide nanoparticles dispersed within the porous activated carbon [9]. We have also developed a performance mathematical model for an electrochemical capacitor based on hydrous ruthenium oxide electrodes, which includes both double layer and surface faradic process [10]. The model indicated that the smaller the particles of the active material the better the performance because of the increased surface area per unit volume or mass.

* Corresponding author. Tel.: +1-803-777-7314; fax: +1-803-777-8265.
*E-mail address*: popov@engr.sc.edu (B.N. Popov).

0378-7753/02/$ – see front matter 
PII: S0378-7753(01)00903-X

Since proton diffusion through the amorphous ruthenium oxide is a necessary step for the redox reaction to occur, the ion transport in the bulk of the oxide is also a critical factor which determines the performance of the active material. Thus, a decrease in particle size of ruthenium oxide should increase the utilization of the active material at high discharge rates due to less dependence of the redox process on proton diffusion in the bulk of the active material.

Colloidal method was used in this study to synthesize amorphous $RuO_2{\cdot}xH_2O$/carbon nanocomposite particles. Carbonate ions and carbon materials with high adsorption ability were used to prevent gelation of sol (colloid) particles and to control the size of the particles. This low temperature colloidal approach ensures nano-size as well as amorphous nature of $RuO_2$ in the composite structure. In this work, the change of capacitance was determined for $RuO_2{\cdot}xH_2O$/carbon nanocomposite materials which were annealed using different heat treatments.

## 2. Experimental

### 2.1. Electrode preparation

$RuCl_3{\cdot}xH_2O$ (39.99 wt.% Ru) and $NaHCO_3$ (Aldrich) were used as precursors to prepare colloidal solution containing ruthenium complex. The ruthenium complex colloidal solution was formed with a slow addition of $NaHCO_3$ into an aqueous $RuCl_3{\cdot}xH_2O$ solution until the pH of electrolyte becomes five. Since, $NaHCO_3$ also stabilizes the colloidal solution, the excess amount of this compound in the solution prevents carbon from adsorbing the colloidal particles. The colloidal particles were adsorbed onto the carbon black (Vulcan XC-72, Cabot Corp.) by adding the carbon particles into the colloidal solution and then stirring the solution for 24 h. In the early stage of reaction, the colloidal particles were small enough to pass through the 0.45 μm filtering membrane. By increasing the reaction time, the particle size increased to the point where it was possible for the particles to be filtered with the membrane. Next, the powder was washed several times with distillated water and annealed in a convection oven at various temperatures for 18 h. The electrode was fabricated as a pellet type (∼10 mg) using 95 wt.% of active material and 5 wt.% PTFE. Next, the pellet was cold pressed between two tantalum grids.

Electrochemical characterization studies were carried out using an EG&G PAR Model 273A. SCE. Pt plates were used as a reference electrode and a counter electrode, respectively. Cyclic voltammograms were obtained by polarizing the working electrode between 0 and 0.9 V in a 1 M $H_2SO_4$ aqueous solution. Transmission electron microscopy (TEM, Hitachi H-8000 model) was used to examine the nanostructured $RuO_2$. X-ray diffraction analysis (XRD, Rigaku 405S5 with Cu $K_\alpha$ as the radiation source) and FT Raman spectroscopy (Dilor model Labram 1B model) were used to characterize the ruthenium oxide. Thermogravimetric analyzer (TGA) was used to measure the degree of hydration. The specific surface area was obtained using BET. To examine the rate capability, the constant current and power discharge were performed using the Arbin battery tester.

## 3. Results and discussion

The XRD patterns of $RuO_2{\cdot}xH_2O$ as a function of annealing temperature are shown in Fig. 1. No discernible peak was detected for the samples annealed below 150 °C which

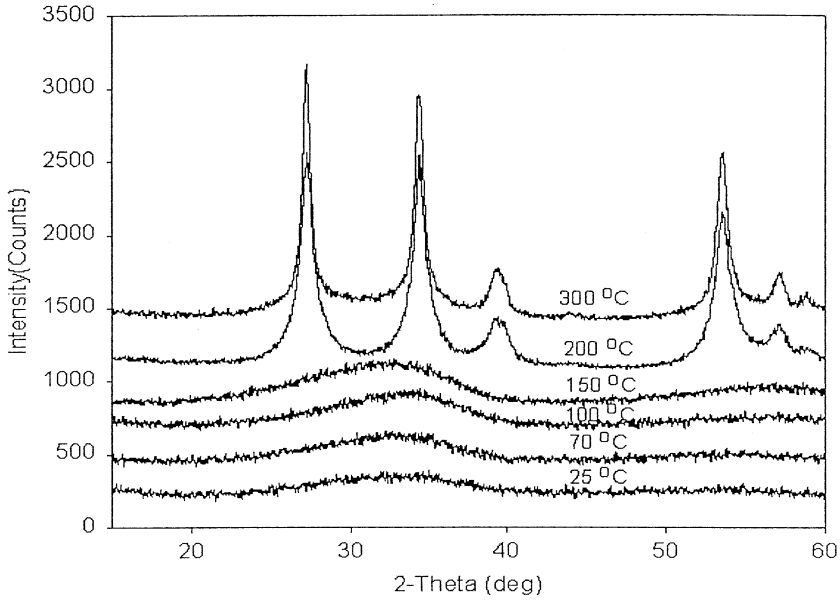


Fig. 1. XRD patterns of pure $RuO_2$ powders at different annealing temperatures.

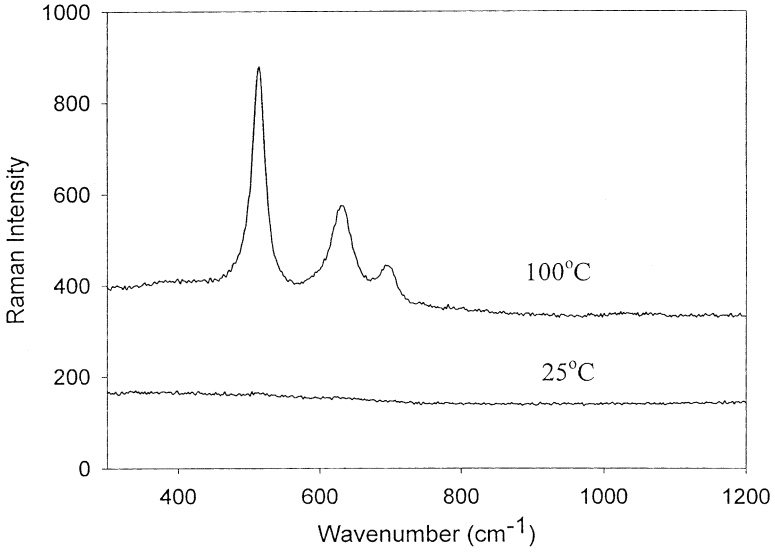


Fig. 2. FT Raman spectra of pure $RuO_2$ powders annealed at 100 and 25 °C.

confirmed the disordered structure of $RuO_2{\cdot}xH_2O$. Sharp diffraction peaks were observed for the samples annealed above 200 °C, which indicated that the amorphous structure of $RuO_2{\cdot}xH_2O$ changed to the crystalline between these temperatures. The results are in agreement with those reported by Zheng and Jow [1].

Since the pseudocapacitance of $RuO_2{\cdot}xH_2O$ is related to the degree of crystalline (the degree of hydration), the annealing process is very critical in optimizing the electrochemical performance of $RuO_2{\cdot}xH_2O$. Also, the pseudocapacitance is maximized only when the transport of electrons and protons in $RuO_2{\cdot}xH_2O$ structure are balanced [11–13].

The FT Raman spectrum was used to identify the material annealed below 150 °C. Fig. 2 presents the FT Raman spectra of $RuO_2{\cdot}xH_2O$ annealed at 100 °C and compared with the sample without a heat treatment. As shown in this figure, the sample which was not temperature treated, did not show any peaks while the annealed sample showed three distinct peaks corresponding to $RuO_2$ [14]. The results indicated that the ruthenium complex derived from sodium bicarbonate solution could be converted to the oxide form after annealing the sample at 100 °C. This temperature is low enough to keep the $RuO_2$ in an amorphous structure.

Fig. 3 shows TEM image of $RuO_2{\cdot}xH_2O$ (40 wt.% Ru) annealed at 100 °C. The dark spot shown in Fig. 3 indicates $RuO_2$ particles adsorbed on the carbon black (Vulcan XC-72). The size of the particles is about 3 nm. The particles appear to be evenly dispersed onto the surface of carbon. This was encouraging since no additional mixing step is necessary when fabricating the electrode. If ruthenium oxide and carbon are physically mixed, the existing large difference of density between them makes it difficult to disperse the ruthenium oxide homogeneously into carbon. Since, the capacitance strongly depends on the amount of $RuO_2$ dispersed, this can cause a wide variation of the performance of the electrodes even in cases when the samples are made from the same batch.

Fig. 4 shows cyclic voltammograms of $RuO_2{\cdot}xH_2O$/carbon electrodes which were annealed at different temperatures. The composite electrodes annealed below 70 °C showed a good initial capacitance. However, they are soluble in a strong acidic medium. As shown in Fig. 5, after several cycles, the sample without heat treatment, almost, completely dissolved in 1 M $H_2SO_4$ aqueous solution. The dissolution stopped when the annealing temperature was raised to 100 °C. The sample annealed at 100 °C showed maximum capacitance. With a continued increase in annealing temperature, a sharp decrease in capacitance was observed when annealed temperatures were raised above 200 °C. The observed sharp decrease in capacitance is due to the formation of crystalline $RuO_2$.

The maximum capacitance for the sol–gel prepared material was obtained after annealing at 150 °C and showed no dissolution [2]. The observed difference may be explained by taking into account that the chemical compositions of the starting material in both studies are different. The difference in composition determines the optimum annealing temperature necessary to obtain a maximum specific capacitance [9].

Fig. 6 shows cyclic voltammograms of $RuO_2{\cdot}xH_2O$/carbon composites prepared with different Ru loadings. The results are compared with those of bare Vulcan XC-72. All CVs presented in Fig. 6 indicated a typical capacitor behavior. The current responses monitored during anodic and cathodic sweep remains almost constant over the entire potential window of 0.9 V and increased proportionally with increasing the Ru loading. The capacitance of carbon is mainly attributed to the charge separation between the electrode and the electrolyte. The Vulcan XC-72 with a surface area of ca. 248 $m^2/g$ had a double layer capacitance of ca. 27 F/g. This is a reasonable value since carbon

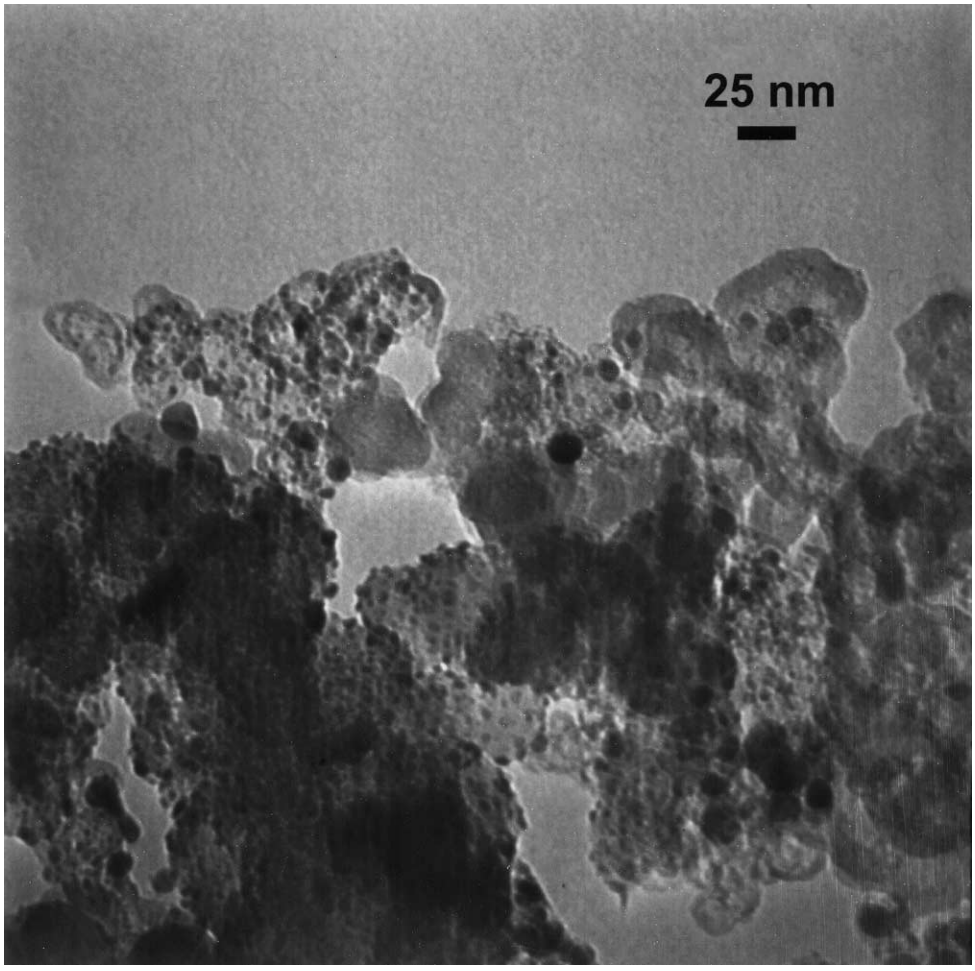


Fig. 3. Transmission electron microscopy of $RuO_2$/carbon composite electrode (40 wt.% Ru) annealed at 100 °C.

materials exhibit a double layer capacitance of 10–30 μF/cm$^2$ in aqueous electrolytes [15,16]. In this study, the carbon with a very low double layer capacitance was selected in order to evaluate with a higher accuracy the $RuO_2{\cdot}xH_2O$ faradic contribution to the overall capacitance of $RuO_2{\cdot}xH_2O$/C composites.

In order to calculate the specific capacitance of $RuO_2{\cdot}xH_2O$ from the total capacitance of $RuO_2$/carbon composite electrode, it is necessary to estimate the amount of $RuO_2{\cdot}xH_2O$ in the electrode. Since, the ratio of Ru/Carbon is known from the amount used to prepare the colloidal solution, the amount of $RuO_2{\cdot}xH_2O$ can be calculated from the change of the molecular weight occurring during the transition to the ruthenium oxide. The hydration number of $RuO_2{\cdot}xH_2O$ annealed at 100 °C was calculated to be 0.55 from the weight change of the samples using TGA analysis. This value is almost the same with the value reported in the literature for active material prepared using sol–gel method [2]. By subtracting the double layer capacitance resulting from carbon from the total capacitance, the specific capacitance of $RuO_2{\cdot}xH_2O$ was estimated to be 863 F/g in case of 40 wt.% Ru loaded electrode (46.3% $RuO_2{\cdot}xH_2O$). The theoretical value of the specific capacitance for $RuO_2{\cdot}xH_2O$ powders is ∼900 F/g [2]. The experimental value of 863 F/g is approximately 96% of the theoretical value.

The specific surface area of $RuO_2$/carbon composite material, the specific capacitance of the composite electrode, the specific capacitance of $RuO_2{\cdot}xH_2O$ considering the contribution of the double layer capacitance from carbon are listed in Table 1 for different Ru loadings. As shown in Table 1, the measured BET surface area of the composite powder for 40 wt.% Ru is 201 m$^2$/g. The value of the specific surface area $a_{BET}$ of $RuO_2{\cdot}xH_2O$ was calculated to be 286 m$^2$/g by using the equation $a_{BET} = (6/D\rho)$, where $D$ is the average diameter of $RuO_2{\cdot}xH_2O$ (estimated by TEM to be 3 nm) and $\rho$ is the mass density of $RuO_2$ (6.97 g/cm$^3$) [17]. By subtracting the surface area of pure $RuO_2{\cdot}xH_2O$ from the measured surface area of the composite powder (46.3% $RuO_2{\cdot}xH_2O$ loaded), the available surface area of carbon in the composite electrode was estimated to be 68 m$^2$/g. This value corresponds to 7.4 F/g of the double layer capacitance of carbon from a total estimated capacitance of the composite electrode of 407 F/g.

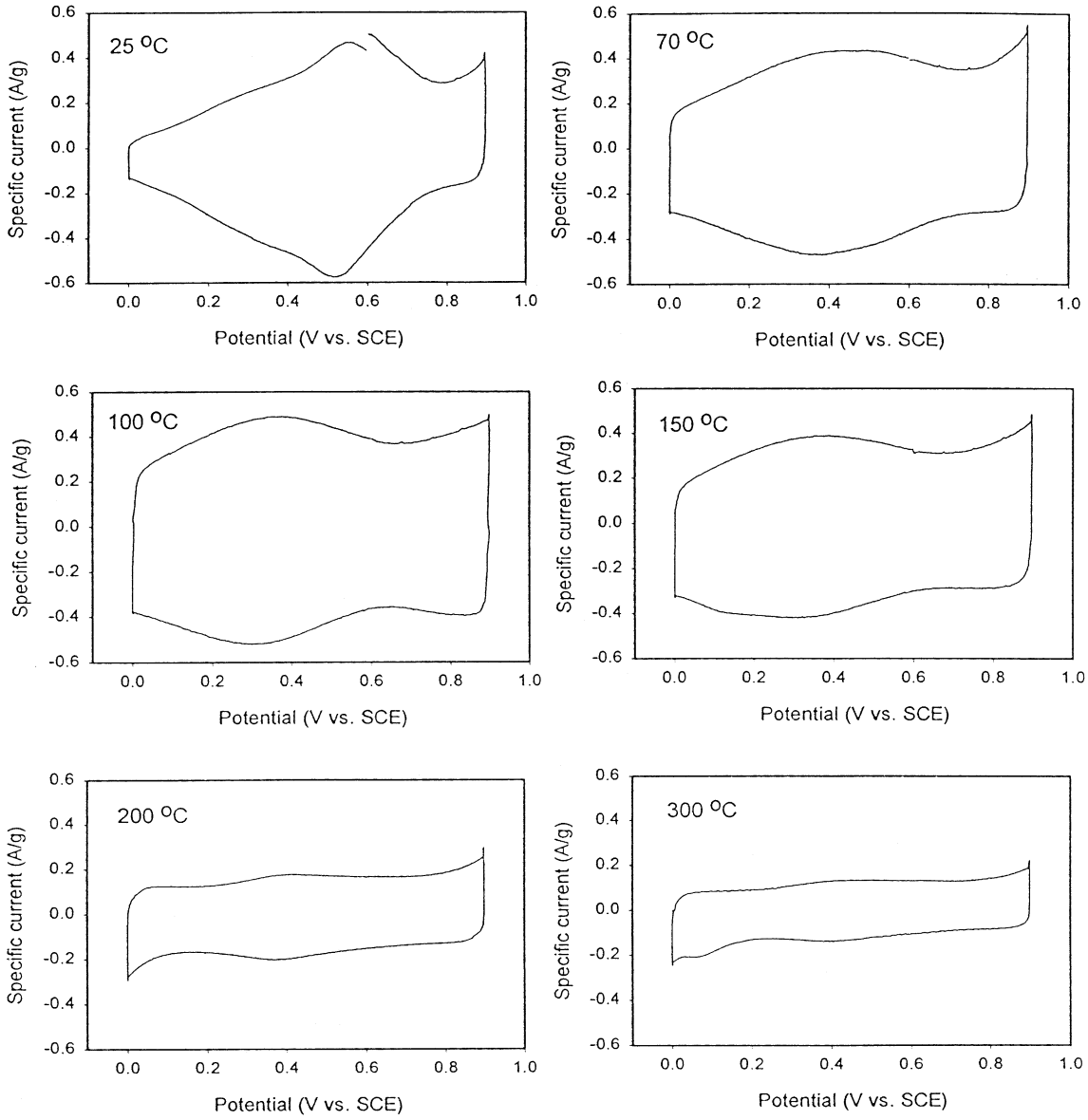


Fig. 4. Cyclic voltammograms of $RuO_2$/carbon composite electrodes (40 wt.% Ru) as a function of the annealing temperatures. Scan rate: 1 mV/s.

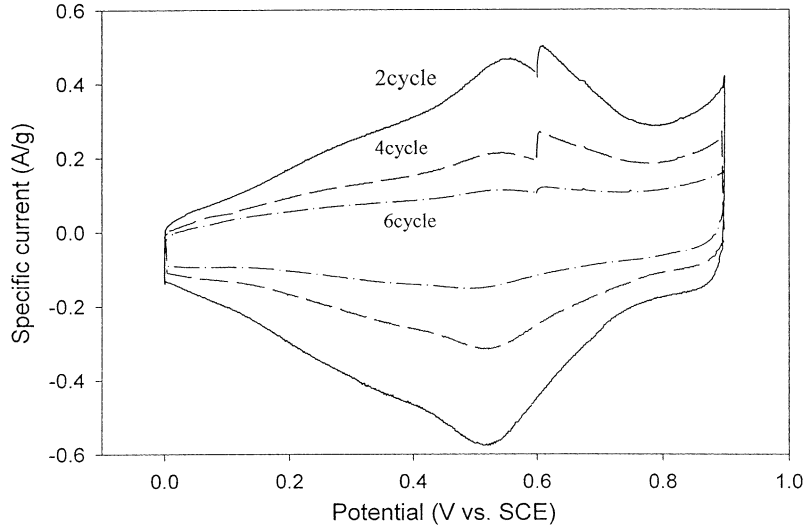


Fig. 5. Stability test of the $RuO_2$/carbon composite electrode (40 wt.% Ru) without annealing process using cyclic voltammograms.

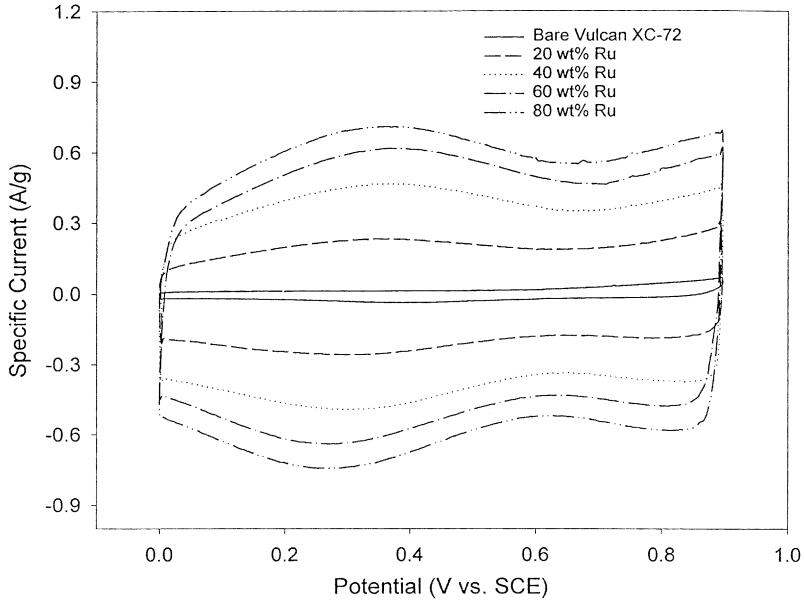


Fig. 6. Cyclic voltammograms of Vulcan XC-72 and different Ru loaded $RuO_2$/carbon composite electrodes in 1 M $H_2SO_4$ electrolyte. Scan rate: 1 mV/s.

The BET data also showed a large difference in the specific surface area estimated for different Ru loadings. The surface area of the composite electrode is composed from the specific surface area of $RuO_2$ and carbon. As shown in Table 1, the specific surface area decreased to 75 $m^2$/g for 80 wt.% Ru loading. This value is almost the same with the specific surface area value of 68.6 $m^2$/g reported in the literature for $RuO_2$ powders prepared by sol–gel technique [2]. Thus, in the case of colloidal method, the specific surface area of $RuO_2$ increases almost three times compared to the sol–gel method, resulting in an increase of the specific capacitance of approximately 11%. By decreasing the particle size of the active material, one increases both the utilization of the active material and its rate capability, as it will be shown later.

By loading $RuO_2$ on carbon, the total weight of the composite increases for a given volume of the material, due to the higher density of $RuO_2$. This results in reducing the BET surface area, since this is normalized to the weight of the active material.

A more useful measure for comparison is to normalize the surface area based on the volume of the composite. Table 1 shows that the volumetric surface area of the $RuO_2$–C composite does not change significantly with the increase in Ru, loading up to 80% indicates that the increase in the weight of the composite does not significantly change the volume. However, as shown in Table 1, the volumetric capacitance of the composite electrode increases much more than the specific capacitance with increased $RuO_2$ loading which is agreement with our previous results obtained for active material synthesized by an electroless deposition process [9].

The specific capacitance of $RuO_2$/carbon composite electrode based on CV curves is presented in Fig. 7. As shown in Fig. 7, increasing the Ru content in the composite, the specific capacitance increased almost linearly. However, after reaching 40 wt.% Ru/C loading, the slope in Fig. 7 decreased indicating that the utilization of $RuO_2$ decreased. The observed decrease in utilization of the active material also shown in Table 1 is due to the change of the particle size of $RuO_2$ particles.

The SEM images shown in Fig. 8 indicated that for 60 and 80 wt.% Ru loaded electrodes, the particle size of $RuO_2$ active materials increased up to several micrometers.

Table 1
BET and capacitance data as a function of Ru loading

| Amount of Ru loaded | Specific capacitance of the composite electrode (F/g) | Specific capacitance of $RuO_2$ alone (F/g) | BET ($m^2$/g) | Volumetric surface area ($m^2/cm^3$) | Volumetric capacity ($F/cm^3$) |
|---|---|---|---|---|---|
| Vulcan XC-72 | 27 | – | 248 | 57.04 | 6.21 |
| 20 wt.% Ru | 221 | 854[a] | 228 | 68.2 | 66.1 |
| 40 wt.% Ru | 407 | 863[a] | 201 | 83.7 | 169.4 |
| 60 wt.% Ru | 526 | 799[a] | 114 | 70.1 | 323.1 |
| 80 wt.% Ru | 599 | 735[a] | 75 | 78.8 | 630.1 |

[a] Considering the contribution of the double layer capacitance from carbon.

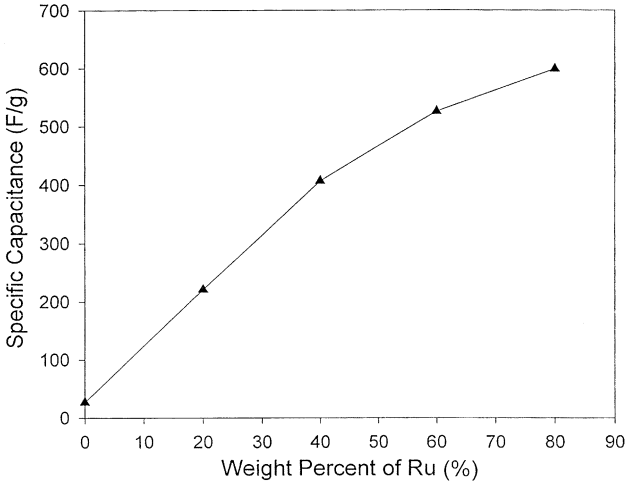


Fig. 7. Specific capacitance of $RuO_2$/carbon composite electrode as a function of Ru loading.

The results in Fig. 7 can be explained by taking into account that the carbon surface available for Ru precipitation at high Ru loadings was not sufficient to accommodate the increased amount of $RuO_2$ particles. Consequently, the Ru particles begin to aggregate, which results in large Ru particles to be precipitated on carbon. Since proton diffusion through ruthenium oxide controls the redox reaction in the bulk of the oxide, the rate capability of this material will decrease with increasing particle size of the oxide. In other words, for the same discharge rate the specific capacitance of $RuO_2$ will decrease in case of larger particle size, since the protons need more time to reach the bulk of the oxide.

The rate capability of $RuO_2$/carbon composite electrode was determined using both the constant current and constant power discharge. Fig. 9 summarizes the electrochemical performance of 40 wt.% Ru loaded electrode at various current densities. Increasing the discharge current density, as expected the capacitance decreased. However, even at very high discharge rate of 400 mA/cm$^2$, high specific capacitance of 277 F/g was obtained.

Fig. 10 presents discharge curves at constant power discharge of 4000 W/kg as a function of Ru loading. As shown in this figure, the potential energy density dependence did not show the same linear behavior as it was observed in the case of a constant current discharge because at constant power discharge the current increases during discharge in order to maintain a constant power load. At high power rate discharge of 4000 W/kg, due to small particle size of 3 nm, the 40 wt.% Ru loaded electrode showed higher energy density than 60 wt.% and even 80 wt.% composite electrode which have particle size of over 1 μm. The results indicated that under high rate operation conditions, 40 wt.% $RuO_2$ loaded composite electrode is more effective and can reduce the material cost by half. Due to low $RuO_2$ loading of 20% in the composite electrode, this electrode as expected showed the lowest energy density.

Similar results were obtained in Fig. 11 which presents the Ragone plots for various constant power discharges. As the power density increased, the energy density showed relatively constant values and suddenly, decreased at a certain applied power level. Note that different decreasing slopes were obtained for 40 and 60 wt.% $RuO_2$ loaded composite electrodes due to the difference in the particle size of the active material in the composite electrodes. The observed change in the slopes mainly results from the increase of particle size rather than from the decrease of the amount of carbon included in the composite. For a 20% change in Ru loading, the slope decreases more for a change in composition from 60 to 80% as compared to change from

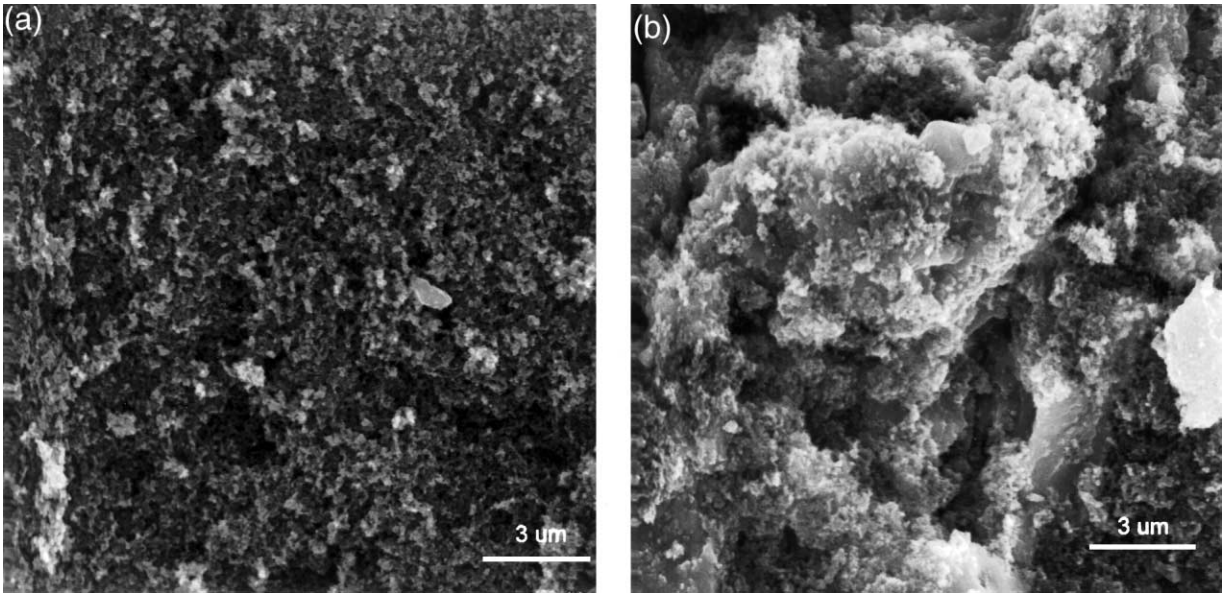


Fig. 8. SEM images of $RuO_2$/carbon composite electrode. (a) 60 wt.% Ru (b) 80 wt.% Ru.

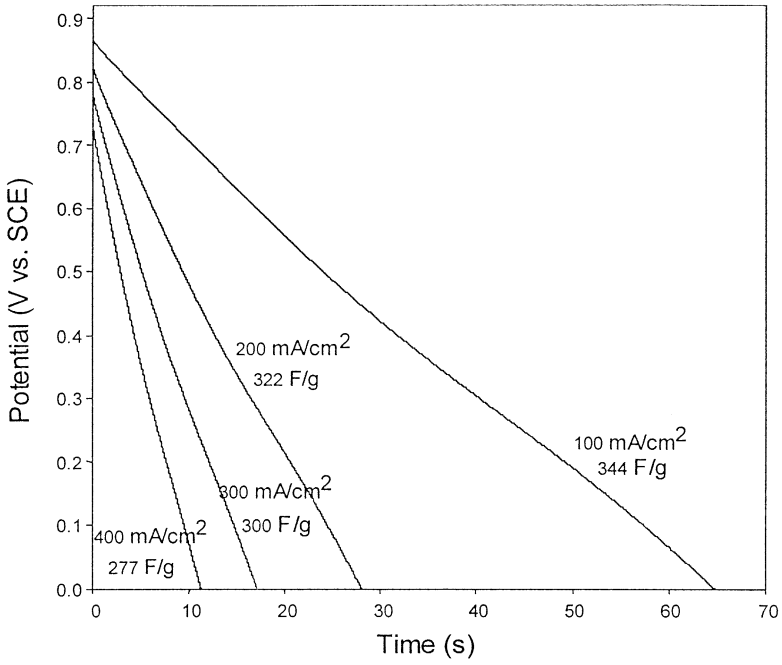


Fig. 9. Electrochemical performance of the $RuO_2$/carbon composite electrode (40 wt.% Ru) with respect to constant current discharge.

20 to 40%. The 80 wt.% Ru loaded composite electrode showed very poor rate capability. This is due to the fact that this composite electrode is composed from large particles. Also, low porosity of this electrode contributes to the poor rate capability because the accumulated $RuO_2$ on the carbon surface blocked most of the pores.

The stability of the active material in the electrolyte was tested using cyclic voltammogram. As shown in Fig. 12, approximately 10% loss of capacitance was observed after 1000 cycles. Most of the capacity fade was observed initially. The results indicated that very stable material has been synthesized using the colloidal method.

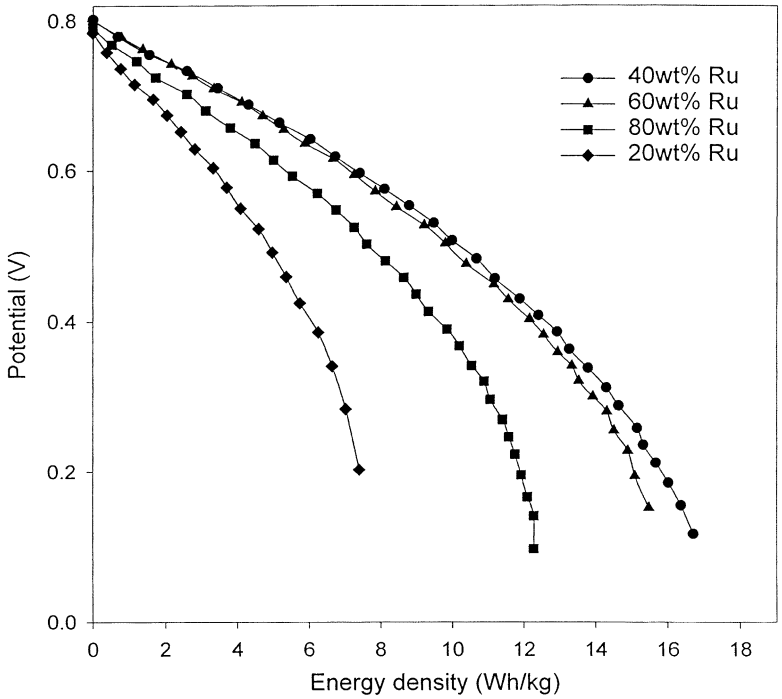


Fig. 10. Discharged energy density curves at the constant power discharge of 4000 W/kg based on the single electrode.

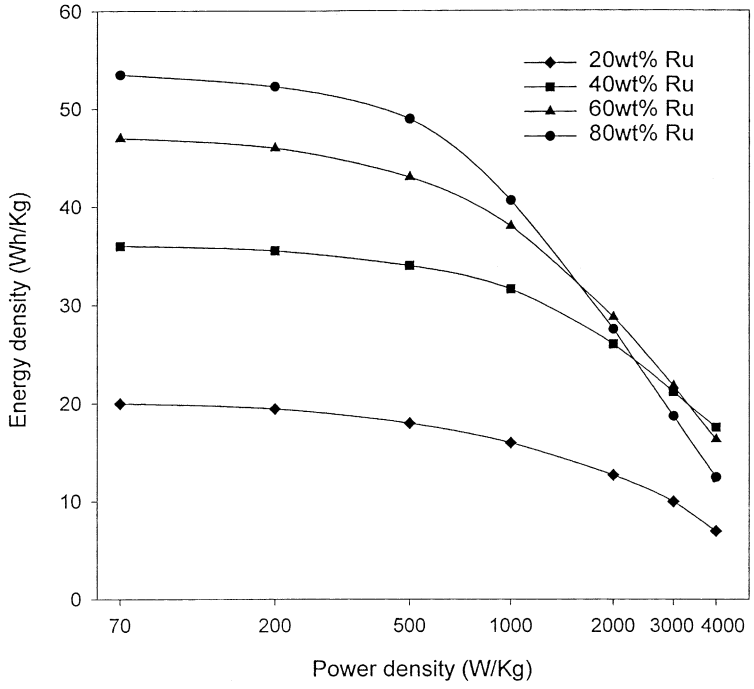


Fig. 11. Ragone plot for $RuO_2$/carbon composite electrode containing different Ru loading.

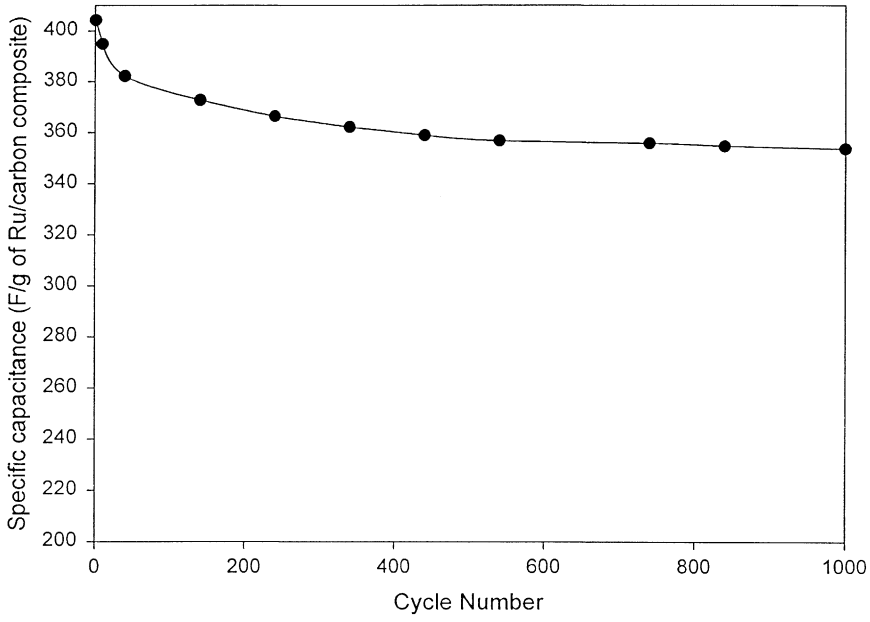


Fig. 12. Cycling behavior of $RuO_2$/carbon composite electrode (40 wt.% Ru). Scan rate: 2 mV/s.

## 4. Conclusion

Amorphous nanostructured composite electrodes based on Ru-oxide were loaded on carbon using colloidal method. The composites were synthesized from solutions containing various amounts of $RuCl_3 \cdot xH_2O$ and $NaHCO_3$ at pH = 5. The electrochemical performance of the composite material depends on the annealing temperature and the particle size of $RuO_2$. Increasing the oxidation temperature above 100 °C increases the crystalline of the deposits. The maximum specific capacitance of $RuO_2$/carbon composite electrode (40 wt.% Ru) was obtained at 100 °C. The particle size of $RuO_2$ was affected by the Ru/carbon weight ratio used to prepare the composite electrode. Transmission electron microscopy indicated that the particle size of Ru is approximately 3 nm in 40 wt.% Ru loaded composite electrode.

Increasing the Ru/C ratio over 40 wt.% resulted in an increase of particle size, which caused a decrease in $RuO_2$ utilization and its rate capability. When constant power of 4000 W/kg was used to discharge the capacitor, the 40 wt.% Ru loaded composite electrode showed 17.6 Wh/kg of energy density. This is a higher value than that estimated for 60 and 80 wt.% Ru loaded composite electrodes.

## Acknowledgements

Financial support by the Commission on Higher Education Fund no 15510-G112 is acknowledged gratefully.

## References

[1] J.P. Zheng, T.R. Jow, J. Electrochem. Soc. 142 (1) (1995) L6.
[2] J.P. Zheng, P.J. Cygan, T.R. Jow, J. Electrochem. Soc. 142 (1995) 2699.
[3] J.P. Zheng, Electrochem. Solid State Lett. 2 (1999) 359.
[4] J.M. Miller, B. Dunn, J. Electrochem. Soc. 144 (1997) L309.
[5] J.M. Miller, B. Dunn, Langmuir 15 (1999) 799.
[6] Y. Sato, K. Yomogida, T. Nanaumi, Y. Ohsawa, M. Kawai, Electrochem. Solid State Lett. 3 (2000) 113.
[7] M. Ramani, B.S. Haran, R.E. White, B.N. Popov, J. Electrochem. Soc. 148 (2001) 374.
[8] M. Ramani, B.S. Haran, R.E. White, B.N. Popov, J. Power Sources. 93 (2001) 209.
[9] C.L. Lin, B.N. Popov, H.J. Ploehn, J. Electrochem. Soc., 2001, in press.
[10] C.L. Lin, J.A. Ritter, B.N. Popov, R.E. White, J. Electrochem. Soc. 146 (1999) 3168.
[11] D.A. McKeown, P.L. Hagans, L.P.L. Carette, A.E. Russell, K.E. Swider, D.R. Rolison, J. Phys. Chem. B 103 (1999) 4825.
[12] J.W. Long, K.E. Swider, C.I. Merzbacher, D.R. Rolison, Langmuir 15 (1999) 780.
[13] J.P. Zheng, T.R. Jow, US Patent 5,961,887 (1999).
[14] J. Haines, J.M. Leger, M.W. Schmidt, J.P. Petitet, A.S. Pereira, J.A.H. Dajornada, S. Hull, J. Phys. Chem. Solids 59 (1998) 239.
[15] K. Kinoshita, Carbon: Electrochemical and Physicochemical Properties, Wiley, New York, 1988.
[16] H. Shi, Electrochem. Acta 41 (1996) 1633.
[17] D.R. Lide (Ed.), CRC Handbook of Chemistry and Physics, 71st Edition, CRC Press, Boca Raton, FL, 1984.